Developmental Cell, Volume *58*

Supplemental information

Epithelial tissue confinement inhibits cell growth and leads to volume-reducing divisions

John Devany, Martin J. Falk, Liam J. Holt, Arvind Murugan, and Margaret L. Gardel

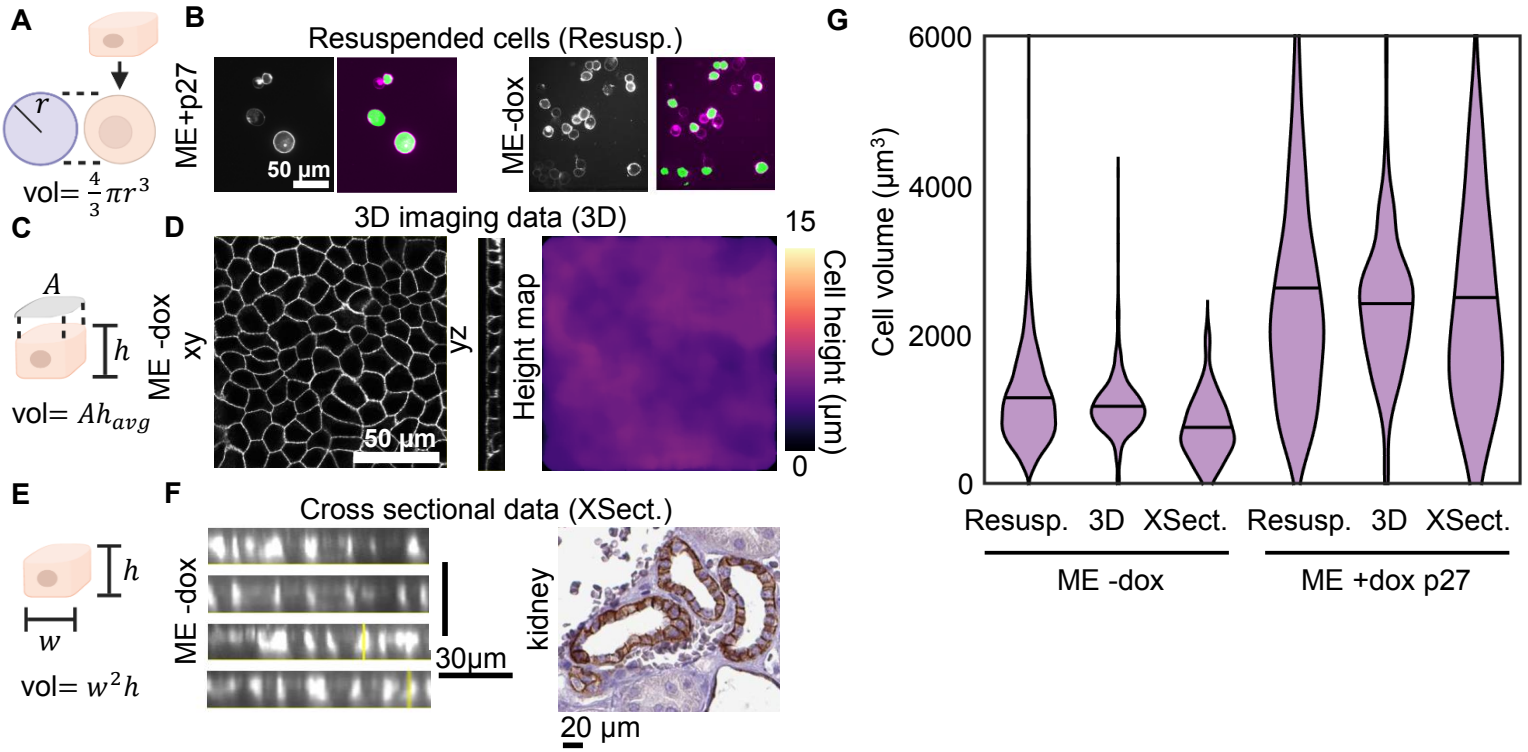

Figure S1. Different volume measurement methods give consistent results, related to STAR Methods

We used several methods to estimate the cell volume across different experiments. While the measurement in 3D is the most accurate method of measuring the cell volume it is not feasible in all experiments. We verified that our other methods of approximation in resuspension and cross section yield the same results as full 3D imaging. (A) Schematic of cell volume measurement in resuspension (Resusp.). The resuspended cell is nearly spherical, and a measurement of the radius is used to determine the cell volume (B) Labeled membranes of resuspendend MDCK cells and corresponding cell segmentation. (C) Schematic of cell volume measurements in 3D – a height map is constructed by measuring the intensity profile at each pixel to identify the top and bottom membrane. The average cell height is multiplied by the cell cross sectional area to obtain the volume (D) 3D z-stack of labeled MDCK cell membranes in XY and YZ views. A height map measured from membranes in the image is displayed and used to measure volume from 2D segmented cell area. (E) schematic cell volume measurements in cross section (XSect.) – cells perpendicular to the imaging plane are identified and the length and width of the cell area measured to estimate the cell volume (F) images of MDCK cell membranes in cross sectional and kidney histology from Human Protein Atlas (image credit: Human Protein Atlas) stained for E-cadherin (CDH1) show cross sectional views of human kidney cells (G) quantification of cell volume using each method for MDCK tet-on P27 cells in ME-dox and ME+dox conditions. n= #cells (N=#exp) (n_{R-}=12641(N=5), n_{3D-}=1405(N=2), n_{Xsect-}=78(N=1), n_{R+}=1136(N=3), n_{3D+}=324(N=2) n_{Xsect+}=59(N=1))

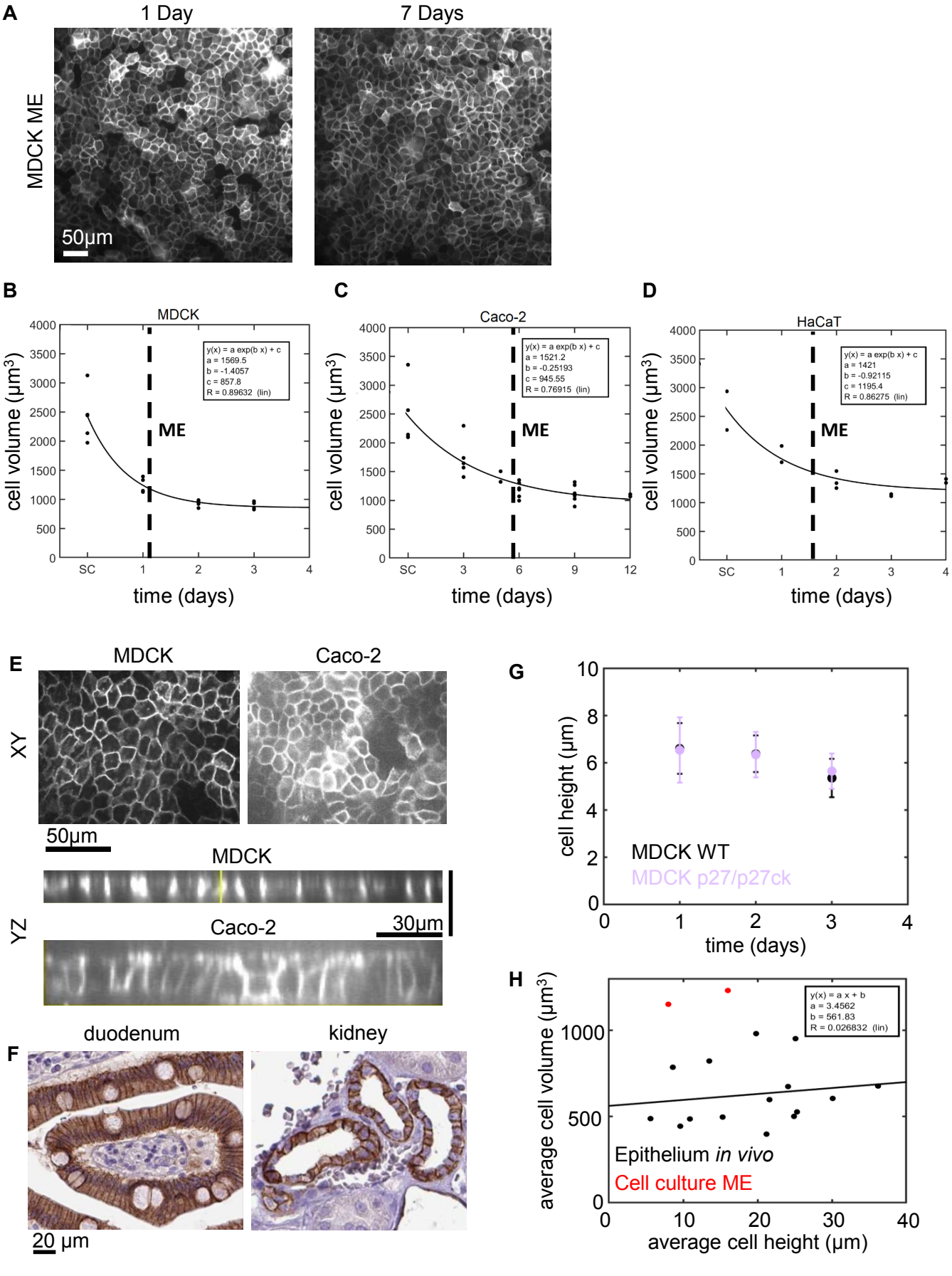
A
1 Day
7 Days
MDCK ME
50µm
B
MDCK
cell volume (µm³)
time (days)
y(x) = a exp(b x) + c
a = 1569.5
b = -1.4057
c = 857.8
R = 0.89632 (lin)
ME
C
Caco-2
y(x) = a exp(b x) + c
a = 1521.2
b = -0.25193
c = 945.55
R = 0.76915 (lin)
D
HaCaT
y(x) = a exp(b x) + c
a = 1421
b = -0.92115
c = 1195.4
R = 0.86275 (lin)
E
MDCK
Caco-2
XY
YZ
50µm
30µm
F
duodenum
kidney
20 µm
G
cell height (µm)
MDCK WT
MDCK p27/p27ck
H
average cell volume (µm³)
average cell height (µm)
y(x) = a x + b
a = 3.4562
b = 561.83
R = 0.026832 (lin)
Epithelium in vivo
Cell culture ME

Figure S2. Cell volume reaches a plateau in mature epithelium (ME) and cell height remains consistent over time for each cell type but varies between tissues, related to Figure 1

We wanted to confirm that in the mature epithelium there are no changes in cell volume. We performed volume measurements across different time points for each cell line and define what time points we consider the system to reach ME by for each cell line. Due to differences in division rates this varies but all cell lines show a decreasing size over time leading to a plateau. Across our dataset we also observed a large variation in cell height. We verified that across experiments and different time points with the same cell line the height remains nearly consistent. We also show that the difference in volume between different cell types is not a consequence of differences in height. (A) MDCK cells with labeled membranes in monolayers imaged at ME+1 day and ME+7 days (B) MDCK cell volume measured in resuspension at different time points (C) CACO-2 cell volume measured in resuspension at different time points. (D) HaCaT cell volume measured in resuspension at different time points. In all experiments t=0 is the onset of confluence. Each point represents the average of >300 cell volumes from a single biological/experimental replicate. In each plot ME is denoted by a dotted line at the time when cell volume has decayed by 80% based on the fits. (E) MDCK and Caco-2 cell membranes showing XY and YZ views of monolayers. (F) Histology section images from Human Protein Atlas (image credit: Human Protein Atlas) of Duodenum and Kidney tissue stained for E-cadherin (CDH1). (G) Cell height of MDCK monolayers across different time points. Data are from 3D segmentation. Error bar shows standard deviation of 20 different fields of view containing >100 cells from 1 experiment each. P27/p27ck are monolayers made from a mixture of Tet-On p27 and Tet-On p27ck cells with doxycycline added at t=0. (H) Plot of cell height vs volume measured in cross section across 15 different tissues *in vivo* analyzed in Fig. 1B and two cell lines cultured as ME *in vitro* (MDCK and CACO-2). Black line shows linear fit to *in vivo* data. Variations in cell height do not explain the variation in cell volume.

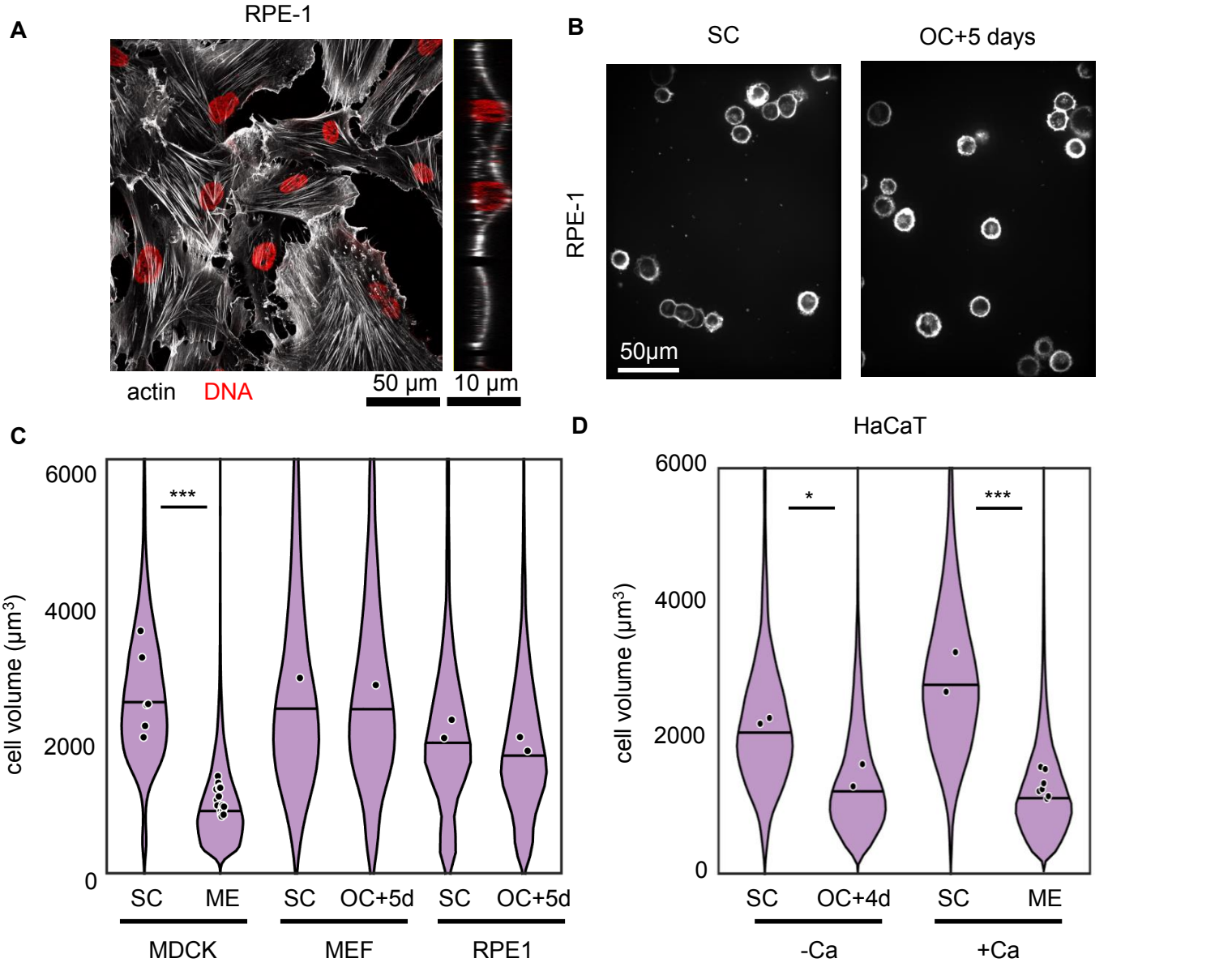

Figure S3. Cell volume does not change during contact inhibition of non-epithelial cells, related to Figure 1

We wanted to determine if the uncoupling of cell growth and division also extends to other cell types which would not form epithelium *in vivo*. We tested two cell lines with fibroblast-like morphology and found that these do not show cell size changes. HaCaT cells are routinely cultured in the absence of calcium which inhibits junction maturation and differentiation, but this did not inhibit cell size reduction in HaCaT cell under confinement. This suggests that the formation of Ca-dependent cell-cell junctions is not required for growth arrest and volume reducing divisions to occur. Future work is required to understand this difference in behavior for epithelial and non-epithelial cells. (A) staining for actin and DNA in retinal pigment epithelial (RPE-1) cells. Cells do not form coherent colonies or show epithelial morphology (B) RPE-1 cells in suspension labeled with CellMask Deep Red from 5 day old cultures plated at low density to remain SC all 5 days or high density to reach OC at day 0. (C) Volume measured in resuspension of MDCK, RPE-1 and mouse embryonic fibroblast (MEF) cells SC and ME-like culture conditions. SC – subconfluent, ME- mature epithelium at day 4, OC+5d- 5 days after the onset of confluence ($n_{MDCK\text{-}SC}$=4940(N=3), $n_{MDCK\text{-}ME}$=12641(N=5), $n_{MEF\text{-}SC}$=1459(N=1), $n_{MEF\text{-}OC5}$=1352(N=1), $n_{RPE\text{-}SC}$=906(N=2), $n_{RPE\text{-}OC5}$=3429(N=2)) (D) Volume measured in resuspension of HaCaT cells in SC and ME cultures with and without calcium. -Ca – 40uM calcium, +Ca – 1.8mM calcium ($n_{SC\text{-}Ca}$=3642(N=2), $n_{OC4\text{-}Ca}$=23996(N=2), n_{SC+Ca}=9248(N=2), n_{ME+Ca}=13451(N=2))

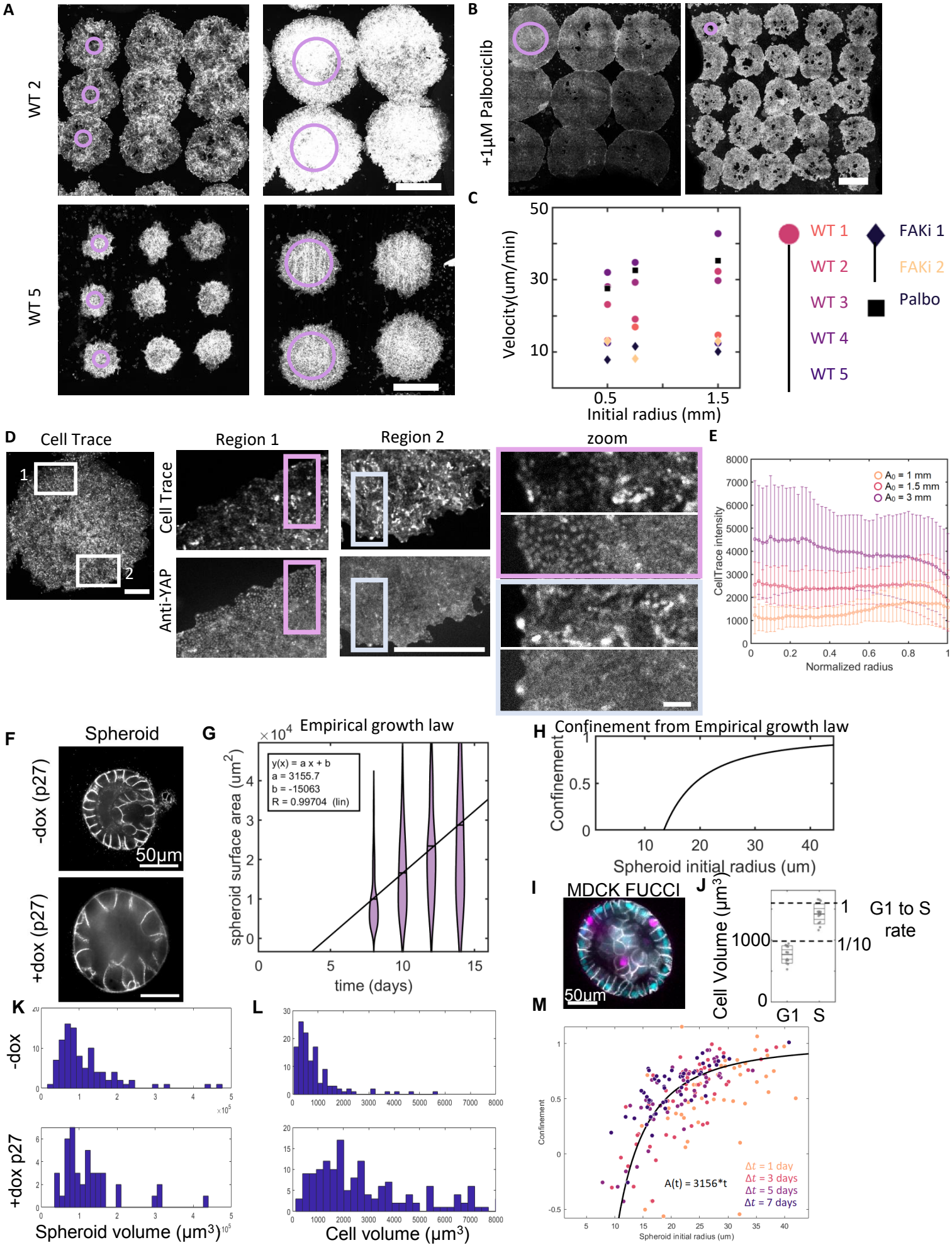
A
WT 2
WT 5
B
+1μM Palbociclib
C
Velocity(um/min)
50
30
10
0.5
1.5
Initial radius (mm)
WT 1
WT 2
WT 3
WT 4
WT 5
FAKi 1
FAKi 2
Palbo
D
Cell Trace
Region 1
Region 2
zoom
1
2
Cell Trace
Anti-YAP
E
A₀ = 1 mm
A₀ = 1.5 mm
A₀ = 3 mm
CellTrace intensity
Normalized radius
F
Spheroid
-dox (p27)
+dox (p27)
50μm
G
Empirical growth law
y(x) = a x + b
a = 3155.7
b = -15063
R = 0.99704 (lin)
spheroid surface area (um²)
time (days)
H
Confinement from Empirical growth law
Confinement
Spheroid initial radius (um)
I
MDCK FUCCI
50μm
J
Cell Volume (μm³)
1
1000
1/10
0
G1
S
G1 to S rate
K
-dox
+dox p27
Spheroid volume (μm³)
L
Cell volume (μm³)
M
Confinement
A(t) = 3156*t
Δt = 1 day
Δt = 3 days
Δt = 5 days
Δt = 7 days
Spheroid initial radius (um)

Figure S4. Colony expansion rate varies between experiments and the confinement framework can also be applied to epithelial spheroids, related to Figure 3

Between different expanding monolayers we observed different migration velocities. We characterized the variation in speed across all experiments and non-uniformity in cell trace intensity. We measured the growth rate of MDCK spheroids and of cells within spheroids to demonstrate another application of our confinement framework. In this context the spheroid expansion is not driven by migration as it is in the expanding monolayers and the growth law is not known. By measuring the behavior of spheroids, we find an empirical growth law and use this to predict the confinement. This confinement agrees with an independent growth measurement on single cells. (A) Expanding colonies labeled with CellTrace Far Red with initial radius 0.5mm and 1.5mm in two different experimental replicates. Migration velocity is consistent within the same experiment but varies between experiments (B) Expanding colonies labeled with CellMask Deep Red treated with 1μM Palbociclib to block cell division. Migration rate is ~30μm/hr equal to the highest rate observed in control conditions. (C) Colony expansion speeds in each experiment for different initial sizes. Expansion occurs for 48 hours and the difference between initial and final radii is used to calculate the velocity. +FAKi is 500nM PND1186. Palbo is 1μM Palbociclib (D) images of expanding monolayers with CellTrace and YAP staining. Zoom in of edge regions highlight growth and signal gradients found close to the edge in some cases. (E) Quantification of the average CellTrace intensity as a function of radius for expanding monolayers. For 3 different experiments 5 expanding monolayers of each initial size were averaged to give the intensity profile as a function of radius. The different experimental averages were averaged to give the points in the final plot. Error bars show standard deviation of the 3 experimental replicates. (F) Distribution of epithelial spheroid size measured at different time points. Linear fit shows the surface area of the spheroid increases with time (G) Confinement as a function of size calculated using the linear growth of spheroid area empirically determined from A (H) Epithelial spheroid of MDCK FUCCI cells with labeled cell membranes (I) Quantification of cell volume of randomly selected cells in G1 and S phase in MDCK spheroids at day 8 (n=13 cells from 1 experiment in each condition). Dotted lines show volumes where the division rate is maximal or 1/10 the maximum from Fig. 5A (J) Representative images of spheroids formed with Tet-On p27 MDCK cells without dox (-dox) or with dox added at t = 5 days. Spheroids were imaged at t = 10 days (K) spheroid volumes in -dox and +dox p27 conditions. Data are from >40 spheroids each in 1 experiment (L) distribution of cell volume in -dox and +dox p27 conditions. Data are from >100 cells each in 1 experiment (M) Measured confinement for individual spheroids from the cell growth averaged across a spheroid measured from changes in cell size under p27 induction compared with the growth model shown in B. Spheroids were grown for 5 days in the absence of dox then dox was added for Δt days. In the presence of dox the cells grow but do not divide. This change in volume can be used to determine the cell growth rate. Cell size in each spheroid is measured after Δt in the presence of dox and compared with the size in -dox conditions ~1000μm^3. The difference in cell size divided by Δt gives the cell growth rate which is compared to the single cell rate of MDCK to give the confinement. The black line represents the confinement calculated in B.

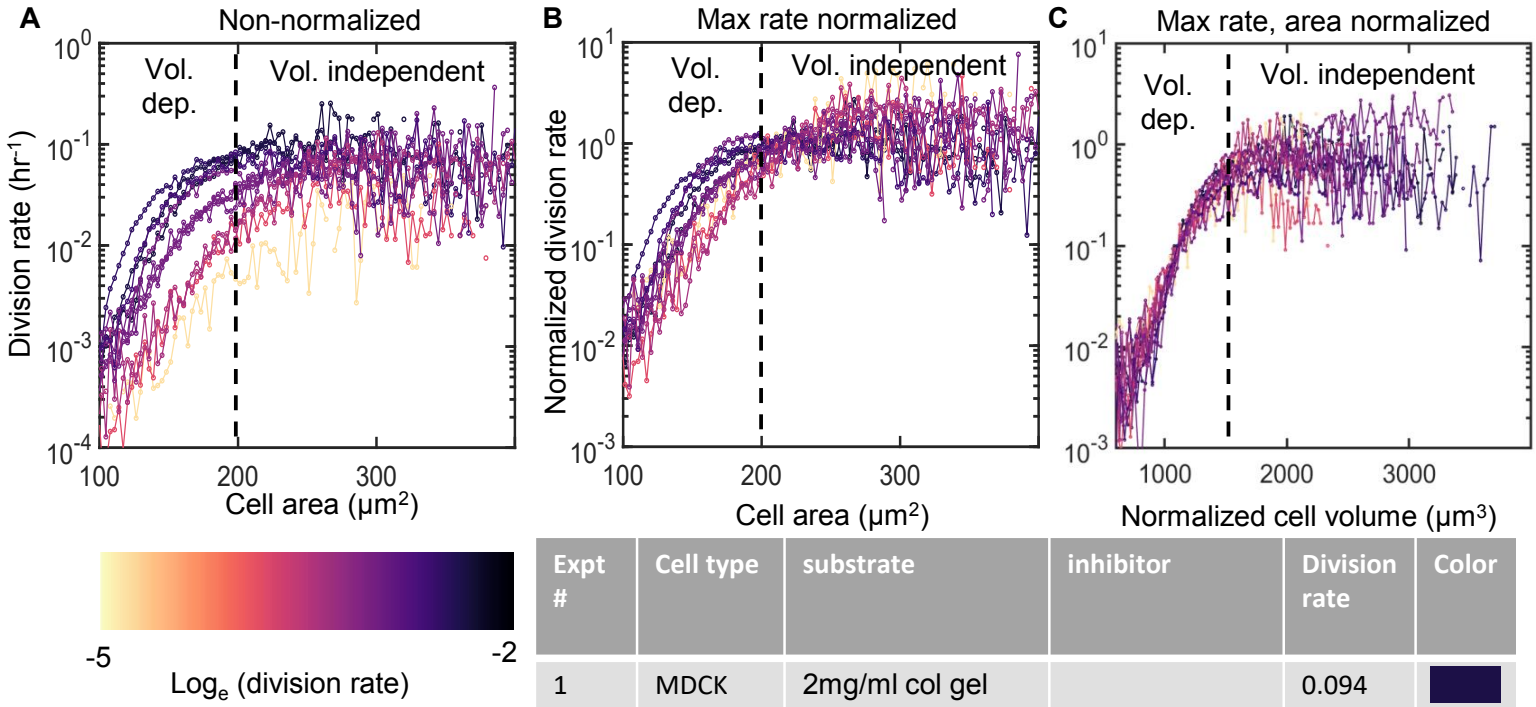

Expt #	Cell type	substrate	inhibitor	Division rate	Color
1	MDCK	2mg/ml col gel		0.094	
2	MDCK	2mg/ml col gel		0.088	
3	MDCK	2mg/ml col gel		0.046	
4	MDCK	2mg/ml col gel		0.067	
5	MDCK	2mg/ml cross linked col gel		0.078	
6	MDCK	4mg/ml cross linked col gel		0.047	
7	MDCK	Glass		0.033	
8	MDCK	2mg/ml col gel	25μM rac inh.	0.048	
9	MDCK	2mg/ml col gel	50μM rac inh.	0.030	
10	MDCK	2mg/ml col gel	500nM FAK inh.	0.022	
11	MDCK	2mg/ml col gel	3um Mn^{2+}	0.046	
12	CACO-2	2mg/ml col gel		0.008	

Figure S5. Cell division rate shows a similar size dependence across a range of experimental conditions, related to Figure 5

We reanalyzed a previously published dataset to see how cell division rates vary with cell size in epithelium. A subset of the data is presented in Fig. 5A but complete set of data analyzed is presented in this figure. We see a consistent relationship between division rate and area despite differences in the overall division rate across experiments. (A-C) Plots of division rates against cell size across 12 timelapse imaging experiments that are previously published by Devany et. al. 2021. Plots show data from 4 replicates of MDCK cells on 2mg/ml collagen gels, data with variation in substrate stiffness, with inhibitors of RAC1 (NSC 23766) and FAK (PND1106), and with CACO-2 cells. See table for full experimental details. Data are plotted non-normalized in A, normalized by the maximum rate in B, and normalized by both maximum rate and the area is normalized so the rate 0.1 is at a volume of 1200 μm^3. Curves are colored according to the maximum division rate. Each division rate curve is generated from tracking >300 division events from each experiment over a timelapse imaging series of at least 16 hours (see Methods). The table lists all conditions that appear in the plots and their respective division rates and serves as a figure legend.

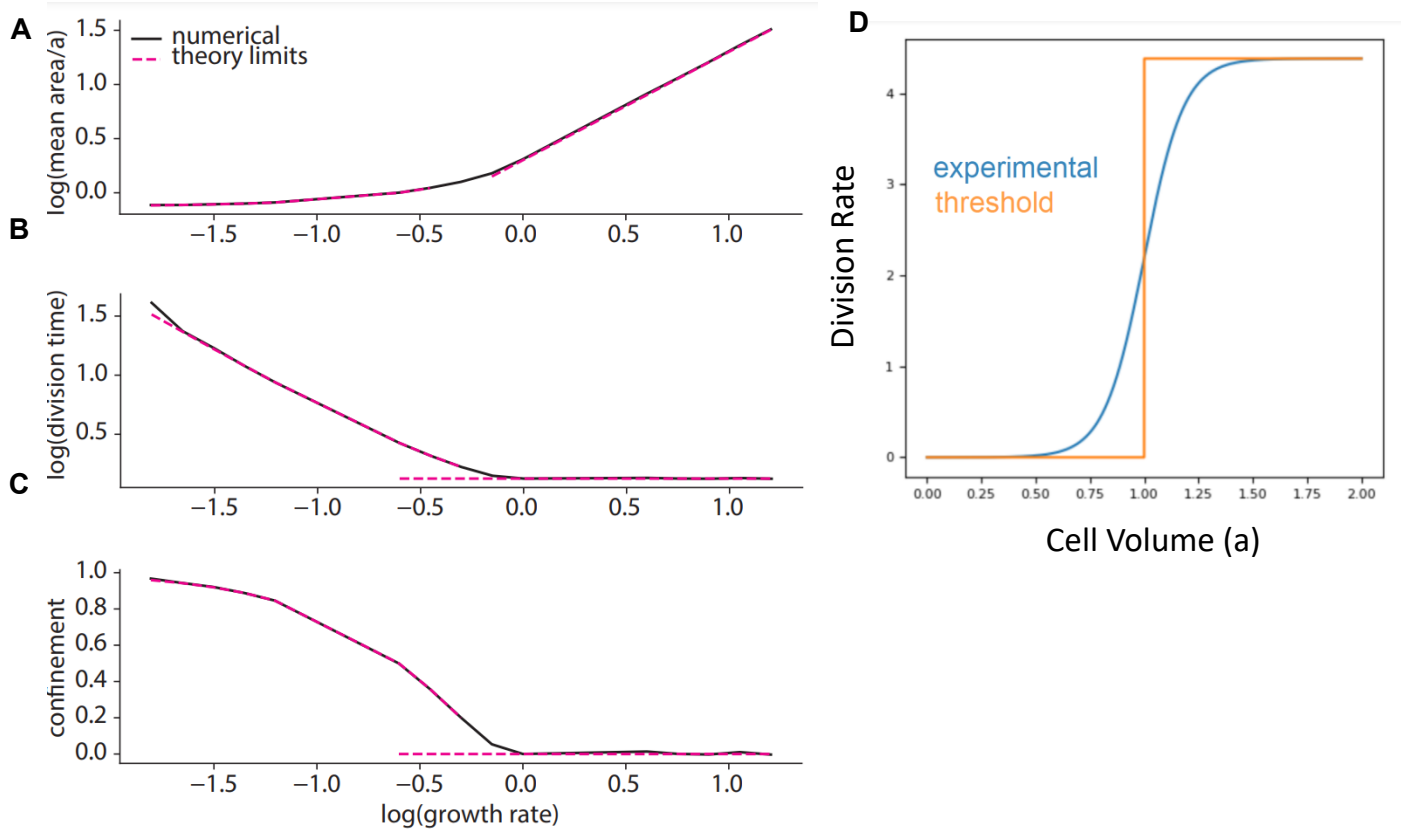
A
numerical
theory limits
log(mean area/a)
B
log(division time)
C
confinement
log(growth rate)
D
experimental
threshold
Division Rate
Cell Volume (a)

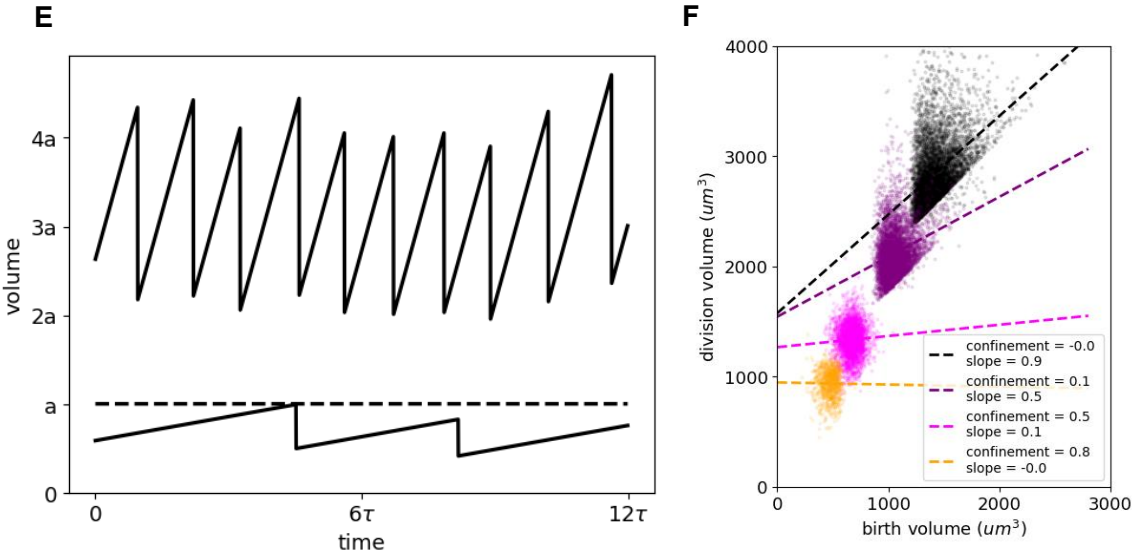
E
volume
time
F
division volume (um³)
birth volume (um³)
confinement = -0.0
slope = 0.9
confinement = 0.1
slope = 0.5
confinement = 0.5
slope = 0.1
confinement = 0.8
slope = -0.0

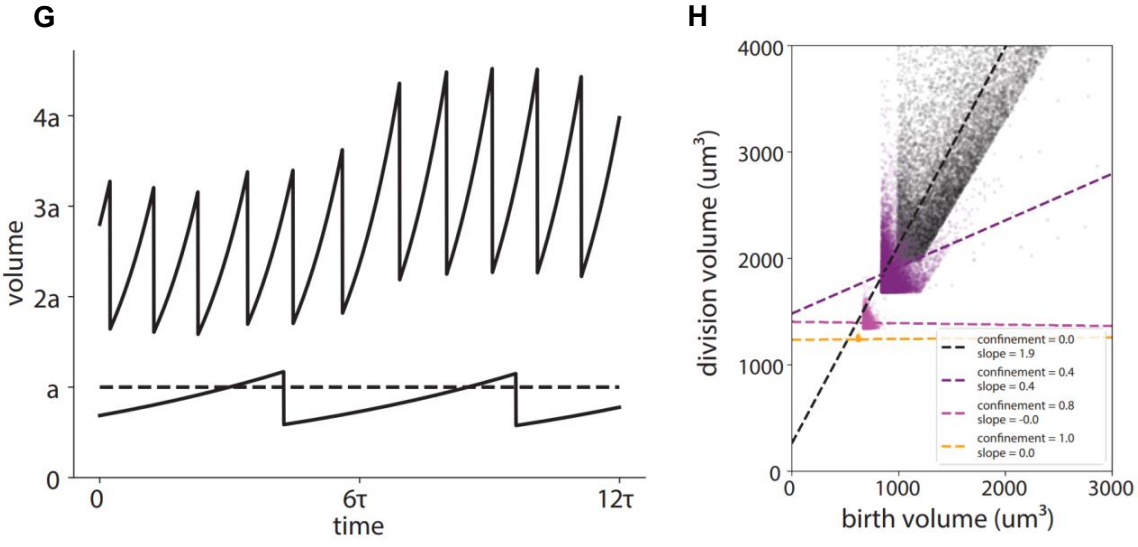
G
volume
time
H
division volume (um³)
birth volume (um³)
confinement = 0.0
slope = 1.9
confinement = 0.4
slope = 0.4
confinement = 0.8
slope = -0.0
confinement = 1.0
slope = 0.0

Figure S6. G1-sizer control generates timer and sizer behaviors depending on growth rate and G1-sizers with modified models of growth and division also transition between timer and sizer behavior, related to Figure 5

We numerically simulate single-cell trajectories (see Methods) as a function of growth rate. We compare our numerical results to analytical expressions (see Methods) derived in the fast- and slow-growth limits of the model. (A) Numerical simulation of mean non-dimensional cell size (black) reveals two distinct regimes: a sizer regime where cell size is only weakly dependent on growth, and a timer regime where size is linear with growth. This agrees well with theoretical expectations in the limits of fast and slow growth (pink). (B) Numerical simulation of mean division time (black) reveals two distinct regimes: a sizer regime where division time diverges with decreasing growth, and a timer regime where division time is independent of growth. This agrees well with theoretical expectations in the limits of fast and slow growth (pink). (C) Numerical simulations (black) reveal a confinement transition when cells switch from sizer to timer behavior: confinement is non-zero for slow-growth sizers, and zero for fast-growth timers. This agrees well with theoretical expectations in the limits of fast and slow growth (pink). (D) To verify that the transition between timer and sizer behavior is not an artifact of our sharp-threshold division rate function, we used a rate function fit from experimental data. This fit (blue) is compared with the threshold (orange) used in Figure 5. We normalize cell volume to the midway point of the fit crossover, and normalize rates to achieve the experimentally observed ratio between average cell cycle length and length of S/G2/M. (E) Numerical simulation of cells with G = 1.8 (upper solid line) and g = .09 (lower solid line) reveals qualitatively distinct timer and sizer behaviors as a function of growth relative to the G1-exit size transition (dashed line). (F) Birth size vs division size correlations reveal a transition from timer/adder-like behavior as a function of confinement. Growth rates G = { 1.0, 0.67, 0.23, 0.05 } going from large to small confinement. (G) To verify that the transition between timer and sizer behavior in our model is not an artifact of linear cell growth, we simulate a model with exponential growth, where cell size a_i increases by an amount a_i*G *dt at each time step. Numerical simulation of cells with G = .74 (upper solid line) and g = .14 (lower solid line) reveals qualitatively distinct timer and sizer behaviors as a function of growth relative to the G1-exit size cutoff (dashed line). The G = .74 trajectory displays the increasing variance of cell size characteristic of timer control with exponential single-cell growth. (H) Plotting numerically simulated cell birth sizes vs division sizes reveals a transition from timer to sizer behavior as a function of confinement. The slope of the linear best fit lines (dotted) to the data goes from timer-like (~2) to sizer-like (~0) as confinement increases. Growth rates G = { 0.5, 0.33, 0.11, 0.025 } going from small to large confinement.

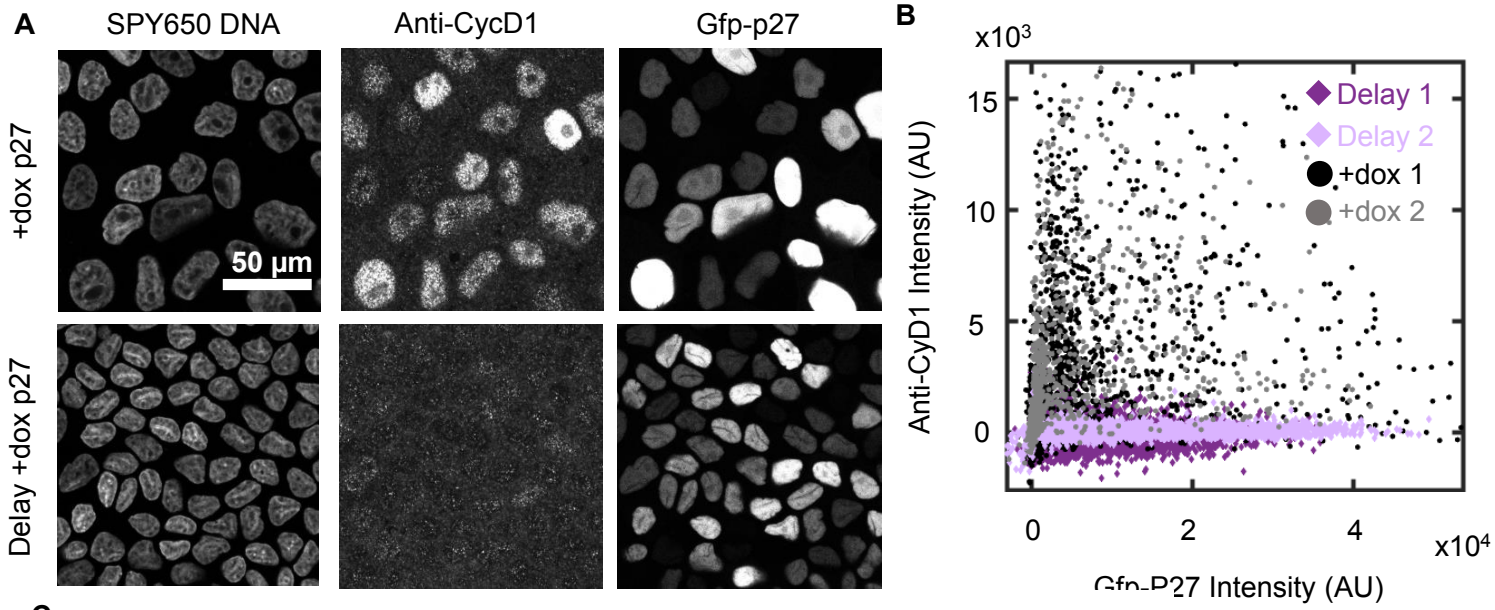

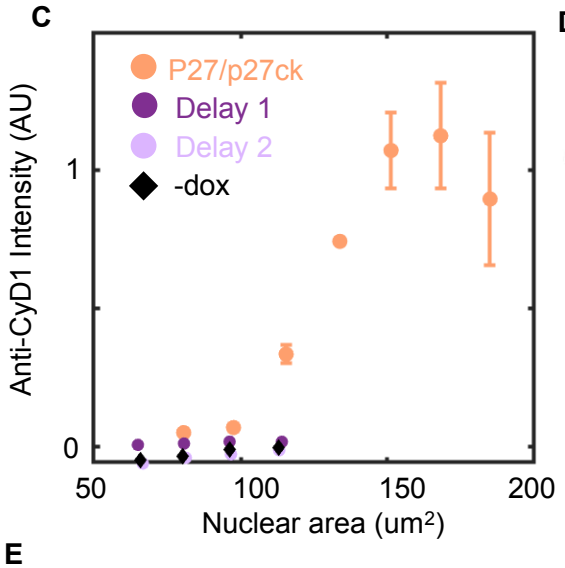

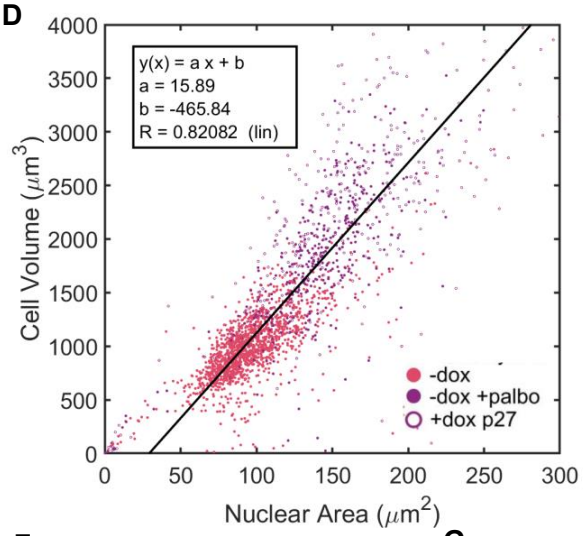

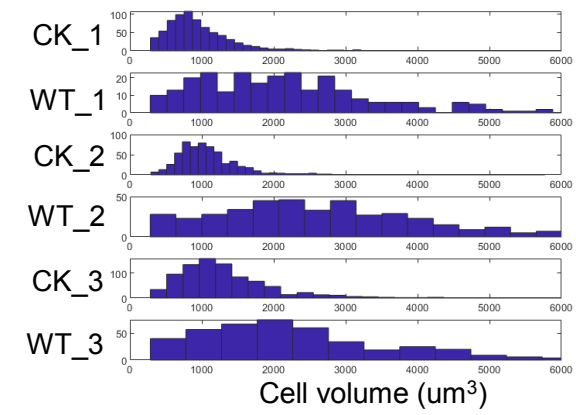

F

TPM

P27-mEmerald	P27ck-snap
0.39268	1166.46
445.51	261.14
11.678	1984.54
455.774	4.95475
1.2774	3499.07
827.005	38.9921

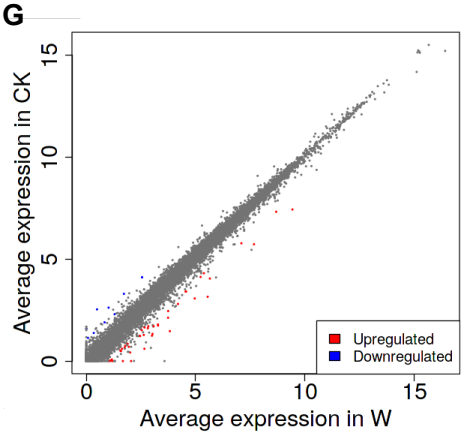

H

Enriched pathways in DEGs for the selected comparison:

Direction	adj.Pval	nGenes	Pathways
Up regulated	5.0e-04	2	MHC class II protein complex assembly
	5.0e-04	3	Antigen processing and presentation of peptide antigen via MHC class II
	5.0e-04	6	Production of molecular mediator of immune response
	1.3e-03	10	Immune response

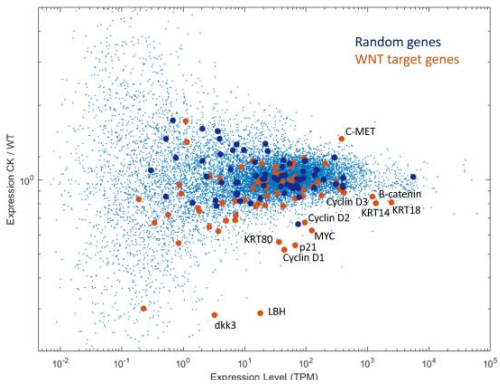

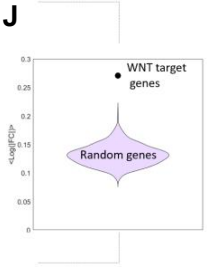

Figure S7. Cyclin D1 level is independent of p27 expression and RNA expression is similar between large and small cells, related to Figure 6

Due to a direct binding interaction between p27 and Cyclin D we were concerned that overexpression of p27 may alter the levels of Cyclin D1 found in normal cells. We performed controls where we manipulate cell size independent of p27 levels and show that there is no resulting effect on expression levels of Cyclin D1. In the cyclin D1 staining experiments, we were restricted to quantifying the nuclear area as a proxy for cell volume. We used 3D imaging data to show that nuclear area serves as a good proxy for cell volume. We also performed RNA sequencing on monolayers with different cell size determined by inhibiting cell division. The data is presented in Fig 6B. This figure includes additional analysis performed on the data which identified some weak transcriptional signatures that we do not interpret to explain the size dependent cell cycle arrest (A) MDCK Tet-On GFP-p27 monolayers labeled with spy650 DNA, anti-cyclin D1 and GFP-p27 under conditions where doxycycline is added at day 0 (+dox p27) or at day 2 (Delay +dox p27) (B) plot of anti-Cyclin D1 nuclear intensity vs GFP-p27 nuclear intensity in +dox P27 or delay +dox P27 conditions (C) Plot of anti-Cyclin D1 nuclear intensity in p27/p27ck coculture, delay +dox p27 and -dox condition. Delay+dox p27 and -dox show similar behavior suggesting that p27 expression does not affect the relationship between Cyclin D1 levels and cell size (n_{+dox1} =1820(N=1) n_{+dox2} = 1112(N=1) n_{Delay1} = 3479(N=1), n_{Delay2} =4036(N=1), n_{-dox} = 4155(N=1) $n_{p27/p27ck}$= 11080(N=4)) (D) plot of nuclear area and cell volume for MDCK tet-on p27 cells cultured as confluent monolayers for 4 days in the presence of absence of doxycycline and Palbociclib (1uM). Cell volumes and nuclear areas were determined by 3D imaging of cells stained with spy650 DNA and JF-546 Halotag labeling stargazin Halotag (n_{-dox}=1405(N=2), $n_{-dox\ +Palbo}$= 390(N=1) $n_{+dox\ p27}$= 324(N=1)) (E) Distributions of cell volumes measured in suspension from each RNA seq experiment (CK – Tet-On Snaptag-p27ck cells +dox, WT – Tet-On GFP-p27 cell +dox). Cells were first synchronized in G1 with Palbociclib for 16 hours, dox was added at t=0 and RNA was collected 5 days later at ME+4 days. 3 samples were made for each experiment and 2 were pooled for RNA extraction and sequencing while the other sample was used to measure the volume distribution (F) expression level of GFP-p27 and Snaptag-p27ck found in each of the samples. Each data set is one experimental replicate with 2 technical replicates. Data show large variations in transgene expression due to experimental variation but show similar phenotypic effects on cell size. (G) Plot of RNA expression from Fig. 6b with genes which are significantly upregulated or downregulated ($P<0.05$) highlighted. Data are averaged from 3 experimental replicates each with 2 technical replicates (H) Pathway enrichment analysis of genes from RNA sequencing data showing all pathways with significant upregulation or downregulation. Analysis performed using iDEP 0.91 (see Methods) (I) plot showing the ratio of gene expression vs the average expression. 65 WNT target genes from The WNT Homepage are plotted in orange while a random set of 65 genes is shown in blue (J) violin plot of average fold change in 1000 sets of 65 random genes compared to the average fold change of WNT target genes in E.

Table S1 - Literature cell size analysis Identifies difference in volume between single epithelial cells and epithelial cells in vivo, related to Figure 1

epithelium in vivo					
tissue	abbreviation	average volume	Standard deviation of volume	cell number	section number
thyroid	Thyr	488.0845	320.3032	104	4
gallbladder	Gall	598.2494	282.3102	87	3
duodenum	Duod	526.9474	279.0266	103	3
stomach	Stom	951.8823	648.3833	105	4
Kidney	Kidn	786.4125	482.418	112	3
small intestine	Sm In	398.2438	225.8594	115	4
mammary	Brea	444.1688	250.3272	106	4
salivary gland	Sa Gl	980.7144	447.0181	96	3
appendix	Appe	605.8217	475.1588	99	4
colon	Colon	501.0309	271.1862	98	3
rectum	Rect	676.8475	376.1879	86	4
endometrium	Endo	673.6342	288.7621	95	3
prostate	Pros	822.1942	536.761	128	3
Fallopian tube	Fa Tu	497.4382	240.5126	96	3
Skin - Basal cells	Skin	485.8623	235.2795	91	3

single cell culture				
line	abbreviation	average volume	reference	figure
HT29-wt	HT2-1	2000	Cadart et al. 2018	fig S2a median delta *1.5
HeLa-hgem	HeL-1	1900	Cadart et al. 2018	fig S2a median delta *1.5
RPE-1	RPE	1300	Cadart et al. 2018	fig S2a median delta *1.5
MDCK-MP	MDC	2600	Cadart et al. 2018	fig S2a median delta *1.5
HT29-hgem	HT2-2	2100	Cadart et al. 2018	fig S2a median delta *1.5
HeLa-MP	HeL-2	3800	Cadart et al. 2018	fig S2a median delta *1.5
HEK293A	HEK	2100	Perez-Gonzalez et. al. 2019, Yao et. al. 2020	fig 1i,k (Perez-Gonzalez) fig 3d (Yao)
HeLa	HeL-3	3300	Guo et. al. 2017	fig 2 on glass
MCF-7	MCF	2300	Leung et. al. 2014	fig 2 average of all sublines
HT29	HT2-3	2300	Park et. al. 2010	fig S3
HeLa	HeL-4	2600	Zhao et. al. 2008	discussion
HiPSc	IPS	1740	Viana et. al. 2021	fig 6b

3D epithelial culture						
line	abbreviation	average volume	reference	figure		
intestine organoid	int-3	1170	de Medeiros et. al. 2021	fig 1f average at 60h		
line	abbreviation	average volume	Standard deviation of volume	cell number	section number	reference
MDCK spheroid	MDC	1024.287	558.5926	89	4	Engelberg et. al. 2011
Caco-2 spheroid	CAC	649.4292	330.473	27	3	Elamin et al., 2012
Intestinal organoids	int-1	621.1405	395.5133	17	3	Goldspink et. al. 2017
Kidney organoid	kid-1	844.5671	532.1591	43	3	Morizane et al. 2015
Intestinal organoids	int-2	827.8124	792.6429	32	2	Karve et. al. 2017
Kidney organoid	kid-2	1765.17	1927.851	33	4	Schutgens et. al. 2019

Table S2: The list of Primers used for cloning and sequencing in this study, related to STAR Methods

All primers we aquired from IDT	
tre3g forward	CACAACACTTTTGTCTTATACTTGG
tre3g reverse	CGGTAGAATTCCATATGACGC
EF-1a Forward	TCAAGCCTCAGACAGTGGTTC
WPRE-R	CATAGCGTAAAAGGAGCAACA
CMVf	CGCAAATGGGCGGTAGGCGTG
BGHrev	TAGAAGGCACAGTCGAGG
gfp p27 f1 fwd	CACTTTTGTCTTATACTTGGATCCATGGTGAGCAAGGGC
gfp p27 f1 rev	GACATAGAGCCACCGCCACCCTTGTACAGCTCGTCCATGC
gfp p27 f2 fwd	GGTGGCGGTGGCTCTAT
tre3g gfp f1 rev	AGAGCCACCGCCACCCTTGTACAGCTCGTCCATGC
tre snap rev	AGAGCCACCGCCACCA
ccnd1 286 AA	cacgtcccgcacgtcggcgggtgcgcaagccaggtccacc
t3g ccnd1 gfp rev	GTAGAATTCCATATGACGCGTTTAgccgatgtccacgtcccgcacgtcgg
ccnd1 gfp fwd	CAAGGGTGGCGGTGGCTCTatggaacaccagctcctgtgc